SECTION 1
INTRODUCTION

Lateral spread on gently sloping ground is generally the most pervasive and damaging type of liquefaction-induced ground failure generated by earthquakes (NRC, 1985). Lateral spread generated by the 1906 San Francisco earthquake damaged several buildings, bridges, roads, and pipelines (Youd and Hoose, 1978). Most notably, lateral spread along Valencia Street between 17th and 18th Street severed water lines to downtown San Francisco. The resulting loss of water greatly hampered fire fighting efforts during the ensuing fire. Lateral spread during the 1964 Alaska earthquake caused $80 million damage (1964 value) to 266 bridges and numerous sections of embankment along the Alaska Railroad and Highway (McCulloch and Bonilla, 1970; Kachadoorian, 1968). Liquefaction and lateral spread also produced widespread damage during the 1964 Niigata, Japan earthquake (Hamada et al., 1986). In Niigata, liquefaction of loose, channel deposits caused the banks of the Shinano River to displace as much as 10 meters toward the center of the channel.

Two general questions must be answered when evaluating the liquefaction hazard for a given site: (1) "Are the sediments susceptible to liquefaction?"; and (2) "If liquefaction does occur, what will be the ensuing amount of ground deformation?" Generally accepted empirical and analytical criteria have been developed to evaluate liquefaction susceptibility (Seed and Idriss, 1971; Seed et al., 1983, 1985; NRC, 1985; Liao, 1986). However, little progress has been made in developing methods for estimating the amount of horizontal ground displacement. This need was noted by the National Research Council in outlining new initiatives in liquefaction research: "Methods of evaluating the magnitude of permanent soil deformations induced by earthquake shaking, while considered in the past, have emerged as a pressing need to understand the dynamic behavior of structures and soil deposits. Both triggering and dynamic soil strength must be considered in studying the effect of liquefaction or high pore pressure on deformations. Calculations based on realistic constitutive models are needed to help comprehend the development of permanent deformations and progressive failure (NRC, 1985, p. 217)."

This paper presents a statistical analysis of liquefaction-induced, ground displacement resulting from lateral spread on gently sloping ground. Multiple linear regression (MLR) is used to develop empirical models from earthquake, topographical, geological, and soil conditions associated with lateral spreads from 8 major earthquakes. The MLR models developed herein provide a means of predicting the amount of horizontal ground displacement at potentially liquefiable sites in earthquake-prone regions.

SECTION 2
LIQUEFACTION, LATERAL SPREAD, AND DISPLACEMENT MODELS

2.1 Liquefaction

In this study, we use "liquefaction" to describe any significant loss of shear strength in a saturated, cohesionless soil due to a transient rise in excess pore pressure generated by strong ground motion. Flow failure, lateral spread, ground oscillation, differential settlement, loss of bearing strength, ground fissures, and sand boils are evidences of excess pore pressure generation and liquefaction.

Unconsolidated fluvial, deltaic, loess, flood plain, fan delta, lacustrine, playa, colluvial, dune, sebka, estuarine, and lagoonal sediments may be moderately to highly susceptible to liquefaction (Youd and Perkins, 1978). Saturated, granular soils found in these depositional environments consist mainly of interbedded layers of loose, sand, silt, and fine gravel. Saturated, poorly compacted, artificial fills are also moderately to highly susceptible to liquefaction (Youd and Perkins, 1978).

Dense, consolidated, or well-cemented, granular soils are not usually susceptible to liquefaction. These soils do not incur significant collapse and pore pressure generation during strong ground motion. Consequently, the loss of shear strength in these soils is negligible. Similarly, liquefaction does not usually occur in nonsensitive, clayey soils. Seed and Idriss (1982) give the following criteria to identify clayey soils that are not normally susceptible to liquefaction: (1) soils with a clay content greater than 15 percent, (2) soils with a liquid limit greater than 35 percent, and (3) soils with a moisture content less than 0.9 times the liquid limit.

2.2 Lateral Spread

Lateral spread is the most common type of liquefaction-induced, ground failure. During lateral spread, blocks of intact, surficial soil displace along a shear zone that has formed within the liquefied layer (Figure 2-1). Upon reaching mobilization, the surficial blocks are transported downslope or in the direction of a free face (i.e., channel or abrupt topographical depression) by earthquake and gravitational forces. Horizontal ground displacement resulting from lateral spread ranges from a few centimeters to several meters. This displacement typically occurs on gentle slopes that range from 0.3 to 5 percent (Youd, 1978). Although, ground displacements as large as 5 to 6 m have occurred on a 0.2 percent slope during the 1964 Niigata, Japan earthquake (Hamada, 1992) and displacements as large as 0.3 m occurred on 0.05 to 0.10 percent slopes during the 1964 Alaska earthquake (Bartlett and Youd, 1992).

Ground deformation resulting from lateral spread typically forms a graben or extensional fissures at the head of the failure, shear deformations along the side margins, and buckling or compression of the soil at the toe. Rigid structures at the head of the failure are commonly pulled apart; those at the toe are compressed or buckled. Buried objects, such as pipelines and piles, are often sheared by differential movement within or at the side margins of the lateral spread.

2.3 Modeling Lateral Spread Displacement

Predicting the amount of ground displacement resulting from dynamic and static forces acting upon a composite system of liquefied and non-liquefied soil is a challenging problem. Ultimately, horizontal ground displacement is controlled by: (1) the degree of shear strength loss in the liquefied layer, (2) the continuity and boundary conditions surrounding the failure, (3) the magnitude and direction of the dynamic and static shear forces acting upon the mobilized soil, and (4) the time interval that these forces exceed the shear strength of the liquefied soil. A rigorous solution of this problem requires a dynamic, 3-D,

analysis of a nonlinear, anisotropic, heterogeneous material.

Several analytical and numerical models have been proposed for calculating liquefaction-induced, ground displacement. However, these models have not been applied to a wide range of earthquake and site conditions. More validation and calibration studies are needed before the practicing engineer can place a high degree of confidence in these techniques.

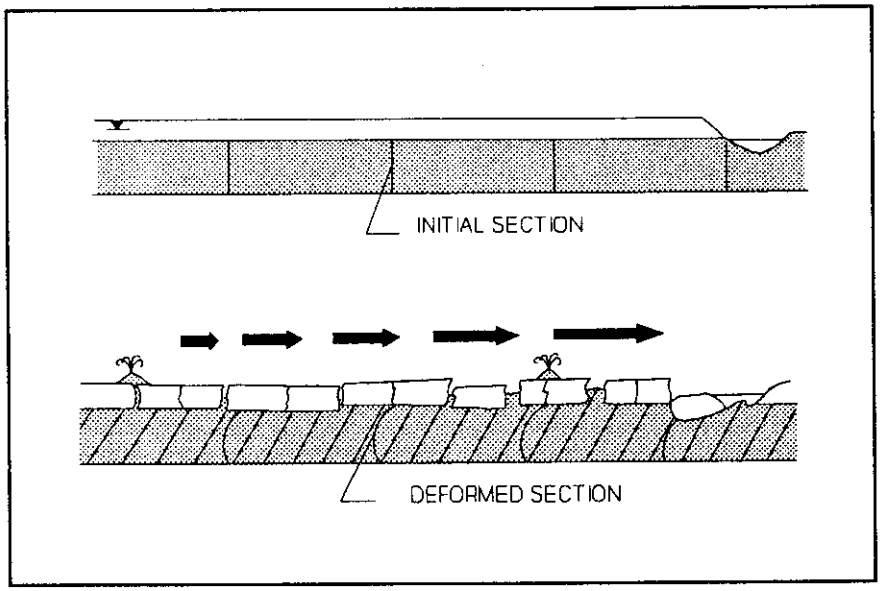

Figure 2-1 Block diagram of a lateral spread before and after failure. Liquefaction occurs in the cross-hatched zone. Surface layer displaces laterally downslope (after Youd, 1984).

2.4 Static Models from Elastic Theory

Hamada et al. (1987), Towhata et al. (1990), and Yasuda et al. (1990) have used static, 2-D, elastic models to estimate the amount of lateral spread displacement resulting from the 1964 Niigata and 1983 Nihonkai-Chubu earthquakes. Hamada et al. (1987) propose that upon reaching liquefaction, the frictional resistance between the liquefied, subsurface layer and the nonliquefied, surface layer approaches zero. The nonliquefied, surface layer is then modeled as a 2-D, elastic beam that is deformed by pre-earthquake, static shear stresses. Likewise, the model proposed by Towhata et al. (1990) treats the nonliquefied, surface layer as an 2-D, elastic beam that is deformed by static shear stresses. The resulting strain is approximated as a sinusoidal curve with zero displacement assigned to the base of the liquefied layer and the maximum displacement assigned at the ground surface. An analytical, closed-form solution is used to calculate the displacement at the ground surface by minimizing the potential energy of the system.

In the first step of a static, 2-D, elastic, finite element procedure proposed by Yasuda et al. (1990), the pre-earthquake, static shear stresses and pre-liquefaction strains are calculated for each element using the elastic modulus of the nonliquefied soil. In the next step, the post-liquefaction strains are calculated for the mesh by holding the pre-earthquake static stresses constant and by reducing the shear modulus of the soil to represent liquefaction. Finally, the strains from the second analysis are subtracted from those of the first to calculate ground displacement vectors.

2.5 Dynamic Models

Prevost (1981), Finn and Yogendrakumar (1989), and Finn (1990) have developed dynamic, 2-D and 3-D models that can be used to predict liquefaction-induced ground displacement. For example in a finite element model, TARA-3FL, proposed by Finn and Yogendrakumar (1989), the pre-earthquake, static, stress-strain state is calculated for each element in the finite-element mesh. In the subsequent, dynamic part of the analysis, as liquefaction is triggered in specific elements according to the criteria developed by Seed (1983) and Seed et al. (1985)., the shear strength of these elements is allowed to drop to its steady-state value.

The post-liquefaction shear strength of these elements is unable to sustain the imposed static and dynamic shear stresses, and the mesh is allowed to progressively deform until equilibrium is restored between the final stress state and the steady-state strength of the liquefied soil. Because deformation can become large, the finite element mesh has to be progressively updated. Calculation of the incremental deformation is done on the current shape of the soil mass and not on the initial shape as in conventional finite element analysis. Finn (1990) also recommends that an static stability analysis be performed on the final soil configuration to verify that the factor of safety is equal to or greater than unity.

2.6 Sliding Block Analysis

Newmark (1965), Goodman and Seed (1966) and Makdisi and Seed (1978), Dobry and Baziar (1990), Byrne (1990), Yegian, et al. (1991), and Mabey (1992) have developed various methods of estimating liquefaction-induced, ground failure displacement from sliding block analysis. In these dynamic, 1-D models, a rigid, soil block is allowed to displace along a planar failure surface during time intervals when the earthquake inertial force, F_{di}, exceeds the yield coefficient of the soil, K_y. The value of F_{di} is calculated by multiplying the horizontal ground acceleration by the mass of the block. Also, F_{di} is assumed to act parallel to the base of the block and is not allowed to vary along the failure surface. K_y is normalized for the weight of the block and is calculated from:

$$K_y = (F_{rs} - F_{da}) / W \qquad (2.6.1)$$

where:
F_{rs} = resisting force due to the dynamic shear strength of the soil
F_{da} = force acting on the block due to active earth pressure
W = weight of the block.

Typically, resisting forces due to irregularities along the failure surface are assumed to be negligible and are omitted from the analysis. Additionally, upslope translation of the block is usually small because the magnitude of the inertial force in the upslope direction seldom greatly exceeds the weight of the downslope component of the soil block.

The net downslope displacement of the block, D_r, is governed by the magnitude and time interval that F_{di} exceeds K_y. Several researchers have proposed solutions for D_r using various shapes for the base input motion. Yegian et al. (1988) have presented solutions for triangular, sinusoidal, and rectangular, base input motions. Franklin and Chang (1977), Makdisi and Seed (1978), Sarma (1979), and Whitman and Liao (1985) have proposed similar solutions for earthquakes of various magnitudes.

As originally introduced by Newmark (1965), sliding block analysis is based on the assumption that the soil within the failure plane deforms as a perfectly plastic material (i.e., F_{rs} remains constant with strain). Many researchers have incorporated the residual strength of the liquefied soil to represent F_{rs} in sliding block analysis. However, the use of a constant value, such as residual strength, to represent the nonlinear, stress-strain behavior of a liquefied soil is a simplification that remains to be validated. In addition, current laboratory and field methods for estimating residual strength are based on limited data and exhibit a great deal of scatter as noted by Marcuson et al. (1990). Thus, the ability of sliding block analysis to accurately predict liquefaction-induced ground displacement may be limited by the uncertainty associated with obtaining representative values of residual strength for the failure surface.

Byrne (1990) has proposed a more sophisticated sliding block model that incorporates shear strength degradation during cyclic loading. Instead of the

rigid-plastic spring proposed by Newmark (1965), a nonlinear spring is used to account for shear strength degradation as liquefaction develops. In Byrne's model, the stiffness of the spring is expressed as a function of both the residual strength and the limiting strain of the liquefied soil. Both of these factors are in turn strongly influenced by the relative density of the cohesionless soil (Seed and Harder, 1990; Seed et al., 1984).

2.7 Empirical Models

Hamada et al. (1986) and Youd and Perkins (1987) have proposed empirical models to predict lateral spread displacement. We will briefly review these models to provide ideas on how earthquake and site conditions can be quantified and used as predictor variables in empirical models.

2.7.1 Liquefaction Severity Index

Youd and Perkins (1987) evaluated cases of liquefaction-induced ground failure that occurred in a very specific geologic setting. They limited their study to lateral spreads that occurred on gentle slopes or into river channels having widths greater than 10 meters. Their study was also restricted to lateral spreads which occurred in saturated, cohesionless, Holocene fluvial or deltaic deposits with estimated standard penetration resistances ranging from 2 to 10 blows per foot. By restricting their study to these site conditions, Youd and Perkins postulated that ground displacement, *S*, becomes primarily a function of the amplitude, A, and duration of strong ground motion, D:

$$S = f(A, D). \qquad (2.7.1.1)$$

Other researchers have shown that A and D are functions of earthquake magnitude, M, and distance from the seismic energy source, R, (Joyner and Boore, 1981; 1988; Krinitzsky and Chang, 1988b). In general, A attenuates logarithmically with R, and D shows a slight increase with increasing R. For many of the lateral spreads in the Youd-Perkins study, strong motion records were not available; thus, they chose to express S as a function of M and log R:

$$S = f(M, \log R). \qquad (2.7.1.2)$$

The moment magnitude, M_w, was chosen to represent M, because it generally provides a better estimate of the total energy released during a seismic event than other measures of earthquake magnitude (Kanamori, 1978).

Youd and Perkins (1987) introduced the "Liquefaction Severity Index" or LSI as a convenient scale to represent the general maximum value of S for a given lateral spread occurring within the defined geological setting. Localities where the reported horizontal ground displacement had obviously exceeded 100 inches (2.5 m) were excluded from the formulation of the LSI equation. Youd and Perkins considered these large displacements to be so damaging and erratic in nature that extending the LSI beyond 100 inches (2.5 m) was not meaningful; thus, the LSI was chosen to range between 0 and 100 inches.

Least squares regression was used to develop the following equation:

$$\log LSI = -3.49 - 1.86 \log R + 0.98 M_w \qquad (2.7.1.3)$$

where:
LSI = maximum, permanent, horizontal displacement in inches (i.e., mm divided by 25)
R = horizontal distance from the energy source in kilometers
M_w = moment magnitude.

Because the LSI equation was developed primarily from lateral spread sites in California and Alaska, it is applicable only to seismic regions with high ground motion attenuation.

2.7.2 Hamada et al. (1986) Equation for Lateral Spread Displacement

Based on pre- and post-earthquake aerial photographs, Hamada et al. (1986) published horizontal ground displacement vector maps for many areas damaged by lateral spreads in Niigata and Noshiro, Japan, during the 1964 Niigata and 1983 Nihonkai-Chubu earthquakes, respectively. Using borehole logs, they also constructed subsurface cross-sections along the longitudinal axis of many of the lateral spreads in these two cities. Guided by changes in the surface topography and breaks in the vector displacement pattern, Hamada et al. divided each cross-section into segments or blocks that appeared to have displaced as a discrete unit (Figure 2-2a and 2-2b). They averaged the displacement vectors, the thickness of the liquefied layer(s), and the slope measurements for each block and used these averages in their correlative analyses.

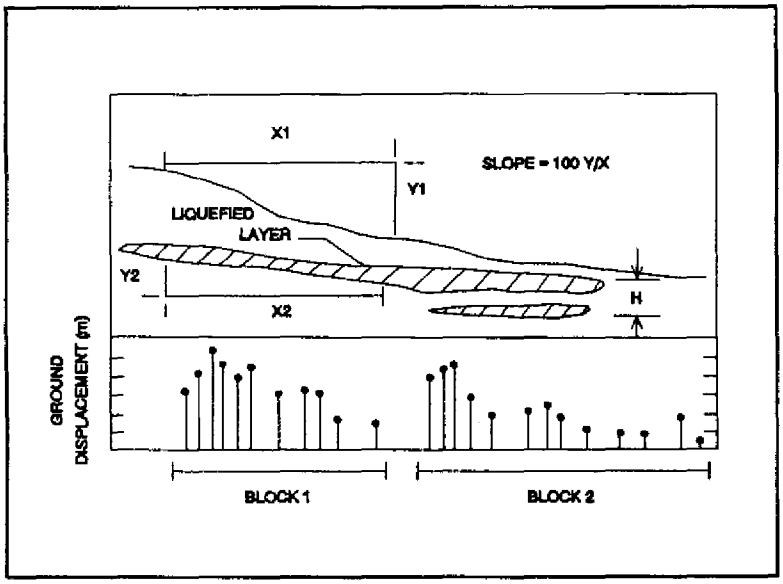

Figure 2-2 (a) Illustration of slope and thickness measurements used in equation 2.7.2.8 (after Hamada et al., 1986).

Hamada et al. used the Factor of Liquefaction Resistance, F_L, to estimate the thickness of the liquefied layer(s), H (Appendix III of Hamada et al., 1986; Iwasaki et al., 1978). F_L is a factor of safety that compares the liquefaction resistance of the soil to the dynamic shear stresses generated by the earthquake:

$$F_L = R/L. \qquad (2.7.2.1)$$

Layer(s) having F_L values less than 1.0 were considered to have liquefied. The in-situ resistance of the soil, R, was calculated from empirical curves adopted by the Japanese Code of Bridge Design. R is a function of the standard penetration resistance of the soil, the effective overburden stress, σ_v', and the mean grain size, D_{50}:

$$R = 0.0882(N/\sigma_v'+0.7)^{1/2} + 0.19 \qquad (2.7.2.2)$$

where:
N = SPT blow count in blows per foot
σ_v' = effective overburden stress in kg/cm^2.

Equation 2.7.2.2 is used for soils with 0.02 mm $\leq D_{50} \leq$ 0.05 mm and Equation 2.7.2.3,

$$R = 0.0882(N/\sigma_v'+0.7)^{1/2} + 0.225 \log (0.35/D_{50}) \qquad (2.7.2.3)$$

is used for soils with 0.05 mm $\leq D_{50} \leq$ 0.6 mm and Equation 2.7.2.4,

$$R = 0.0882(N/\sigma_v'+0.7)^{1/2} - 0.5 \qquad (2.7.2.4)$$

is used for soils with 0.6 mm $\leq D_{50} \leq$ 1.5 mm. The dynamic earthquake shear stress, L, is normalized for σ_v' and is given by:

$$L = 0.65(\sigma_v/\sigma_v')r_d \qquad (2.7.2.5)$$

where:
r_d = a stress reduction factor that reduces L with depth.

Hamada et al. identified the liquefied layer(s) in each cross-section by using F_L. Layers with F_L values less than 1.0 were marked as having liquefied. Boundaries for liquefied layers were interpolated between bore holes to construct a continuous profile along the longitudinal axis of the lateral spread. If liquefaction was indicated in more than one layer, the total thickness of the liquefied layer, H, included the combined thickness of liquefiable layers plus the thickness of any intermediate nonliquefiable layer(s) (Figure 2-2a).

Hamada et al. also estimated the ground slope along the longitudinal axis of each displaced block and correlated it with ground displacement. The ground slope, θ_1, (%), was defined simply as:

$$\theta_1 = 100(Y_1/X_1) \qquad (2.7.2.6)$$

where:
Y = vertical change in surface elevation across the block
X = length of the block (Figure 2-2a).

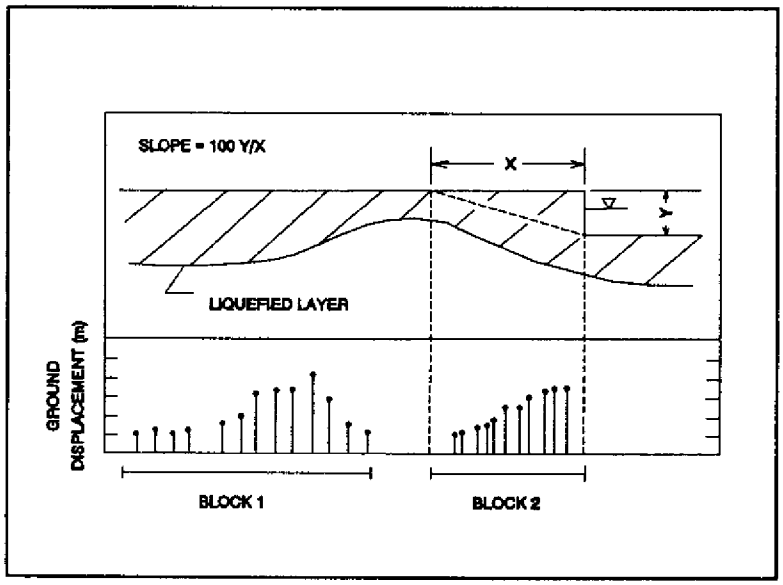

Figure 2-2 (b) Technique used by Hamada et al. to measure the ground slope for lateral spreads along the Shinano River (after Hamada et al., 1986).

For lateral spreads that occurred near the banks of the Shinano River, the measurement of θ_1 was artificially steepened to the bottom of the river channel (Figure 2-2b).

Hamada et al. also postulated that the slope of the bottom of the liquefied layer may have influenced horizontal displacement. This slope, θ_2, (%), was measured by scaling the slope of the bottom of the liquefied layer from the constructed cross-section (Figure 2-2a):

$$\theta_2 = 100(Y_2/X_2). \qquad (2.7.2.7)$$

where:
Y_2 = vertical change in subsurface elevation across the block
X_2 = length of the block.

Hamada et al. found that MLR models which included H in conjunction with the larger value of either θ_1 or θ_2 yielded the best predictions of horizontal displacement. They proposed the following regression model:

$$D = 0.75\ H^{0.50}\ \theta^{0.33} \qquad (2.7.2.8)$$

where:
D = horizontal ground displacement, (m)
H = thickness of the liquefied layer, (m),
θ = the larger value of θ_1 or θ_2, for the block, (%).

Figure 2-3 is a plot of observed displacements from Niigata and Noshiro, Japan, plotted against displacements predicted by this model. Predictions that fall on or near the 45 degree solid line are closely approximated by the model. The dashed line below the 45 degree solid line represents a 100 percent overprediction bound (i.e., the predicted displacements are 2 times larger than observed displacements). The dashed line above the 45 degree solid line represents a 50 percent underprediction bound (i.e., the predicted displacements are one-half times larger than the observed displacements). Approximately 80 percent of the displacements predicted by the Hamada et al. model fall between these two prediction bounds.

2.7.3 Summary of Empirical Models

The LSI equation of Youd and Perkins (1987) is based primarily on earthquake factors and is intended to provide a conservative upper bound for estimating horizontal ground displacement at sites having a moderate to high liquefaction susceptibility. In contrast to the LSI equation, the model proposed by Hamada et al. (1986) emphasizes the thickness of the liquefiable layer and slope, but it does not address the importance of earthquake factors. This thickness-slope model appears to produce reasonable estimates for M ≈ 7.5 earthquakes and for highly liquefiable sediments that are located approximately 20 to 30 km from the seismic source. However, it yields less reliable results for smaller or larger seismic events occurring at varying distances (Bartlett and Youd, 1990). Additionally, the characteristics of the liquefied deposits in Niigata and Noshiro cities are relatively homogeneous (i.e., uniform, medium-to fine-grained, clean sand). Extrapolation of the regression equation to gravelly and silty sediments yields poorer predictions (Bartlett and Youd, 1990).

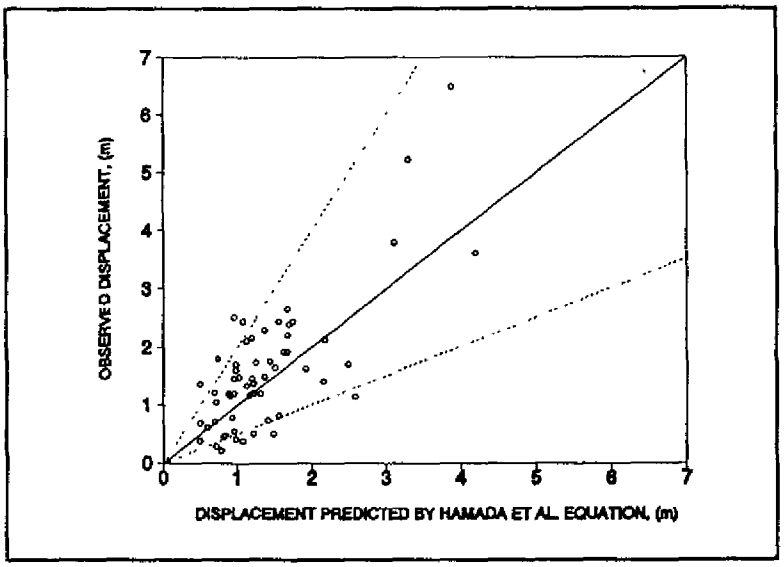

Figure 2-3 Observed displacements plotted against displacements calculated from Equation 2.7.2.8 (after Hamada et al., 1986).

2.7.4 Towards a More Comprehensive, Empirical Model

It is difficult to quantify and model all factors that contribute to liquefaction and ground displacement. Thus, the modeler is forced to select only a handful of the most influential factors and attempt to represent their complex interaction. Based on the studies by Hamada et al. (1986), Youd and Perkins

(1987), and Bartlett and Youd (1990), we believe that a more compressive empirical model should include, but not be restricted to the following: (1) earthquake factors (e.g., peak ground acceleration and duration of strong ground motion or earthquake magnitude and distance from the zone of seismic energy release), (2) topographical factors (e.g., ground slope and/or the distance to and height of a free face, if present), (3) geological factors (e.g., thickness of and depth to the liquefied layer), and (4) soil factors (e.g., residual strength, mean grain size, and the silt and clay content of the liquefied soil).

SECTION 3
EMPIRICAL ANALYSIS OF LATERAL SPREAD FOR NIIGATA AND NOSHIRO, JAPAN

3.1 Multiple Linear Regression

Multiple linear regression (MLR) is often used to predict the behavior of complex phenomena that are influenced by several factors (Draper and Smith, 1981). In applying MLR analysis, it is assumed that changes in the independent variables, **X(s)**, are accompanied by a corresponding change in the response of the dependent variable, **Y**. The true response, $\cap$, is expressed in terms of an unknown function, ϕ, which contains the **X(s)**, and the unknown parameters, **B(s)**, that accompany the **X(s)**.

$$\cap = \phi(X_1, X_2, \ldots, X_p; B_1, B_2, \ldots, B_p) \qquad (3.1.1)$$

For example, in this study we postulate that horizontal ground displacement is a function of several independent variables.

$$\cap = \phi(E, G, T, S; B_E, B_G, B_T, B_S) \qquad (3.1.2)$$

where:
E = Earthquake factors
G = Geological factors
T = Topographical factors
S = Soil factors
B_E, B_G, B_T, and B_S = unknown parameters corresponding to **E**, **G**, **T**, and **S**

Ideally, the value of $\cap$ for a given set of **X(s)** is the same each time the experiment is performed. But, in reality, $\cap$ is seldom observed due to the presence of many uncontrolled and unmeasured variables that affect $\cap$. The deviation of the observed response, **Y**, from $\cap$ is called experimental error, ϵ.

$$\cap - Y = \epsilon \qquad (3.1.3)$$

In MLR analysis, ϕ is approximated by an additive, linear model. The values of **Y** and the **X(s)** are often transformed (e.g., 1/X, log X, e^x, etc.) in order to produce a linear form.

$$Y = b_0 + b_1X_1 + b_2X_2 + \ldots + b_pX_p + e \qquad (3.1.4)$$

The regression coefficients, $b_0, \ldots, b_p$ are best-fit estimates of the **B(s)**, and **e** is a best-fit estimate of ϵ. The method of ordinary least squares is commonly used to estimate the **B(s)** by minimizing the error sum of squares:

$$S_e = \Sigma(e)^2 \qquad (3.1.5)$$

where:
e = difference between the measured response, **Y**, and the response predicted by the regression equation, Y_{hat}, i.e.,

$$e = Y - Y_{hat}. \qquad (3.1.6)$$

To provide these best-fit estimates, it is assumed: (1) the ϵ**(s)** are random variables with an expected value of zero (i.e., $E(\epsilon) = 0$), (2) the variance of the ϵ**(s)** is constant for all values of the **X(s)** (i.e., $V(\epsilon)$ is constant), (3) the ϵ**(s)** are not correlated, and (4) the values of the can be measured without error. Also, if the ϵ**(s)** appear to be normally distributed, then partial and sequential t and F tests can be performed on each of the **b(s)** to verify that these coefficients are statistically significant (i.e., $b_0, \ldots, b_p$ are not equal to

zero) (Draper and Smith, 1981). Standardized residual plots are commonly used to evaluate the validity of these assumptions. Also, these plots give the investigator valuable information about the general performance of the MLR model. The standardized residual, e_s, for each observation is calculated from:

$$e_s = e/(\text{standard deviation of } e) \qquad (3.1.7)$$

where:
$e = Y - Y_{hat}$.

Typically, the $e_s(s)$ from the model are plotted against the corresponding $X(s)$ and $Y_{hat}(s)$ to confirm that the $e_s(s)$ are independent and have a constant variance with a mean of zero. An acceptable standard residual plot gives the impression of a horizontal band of data centered on zero. Approximately 95 percent of the $e_s(s)$ should fall within ± 2 standard deviations of zero, and almost all $e_s(s)$ should fall within ± 3 standard deviations of zero line shown in Figure 3-1a.

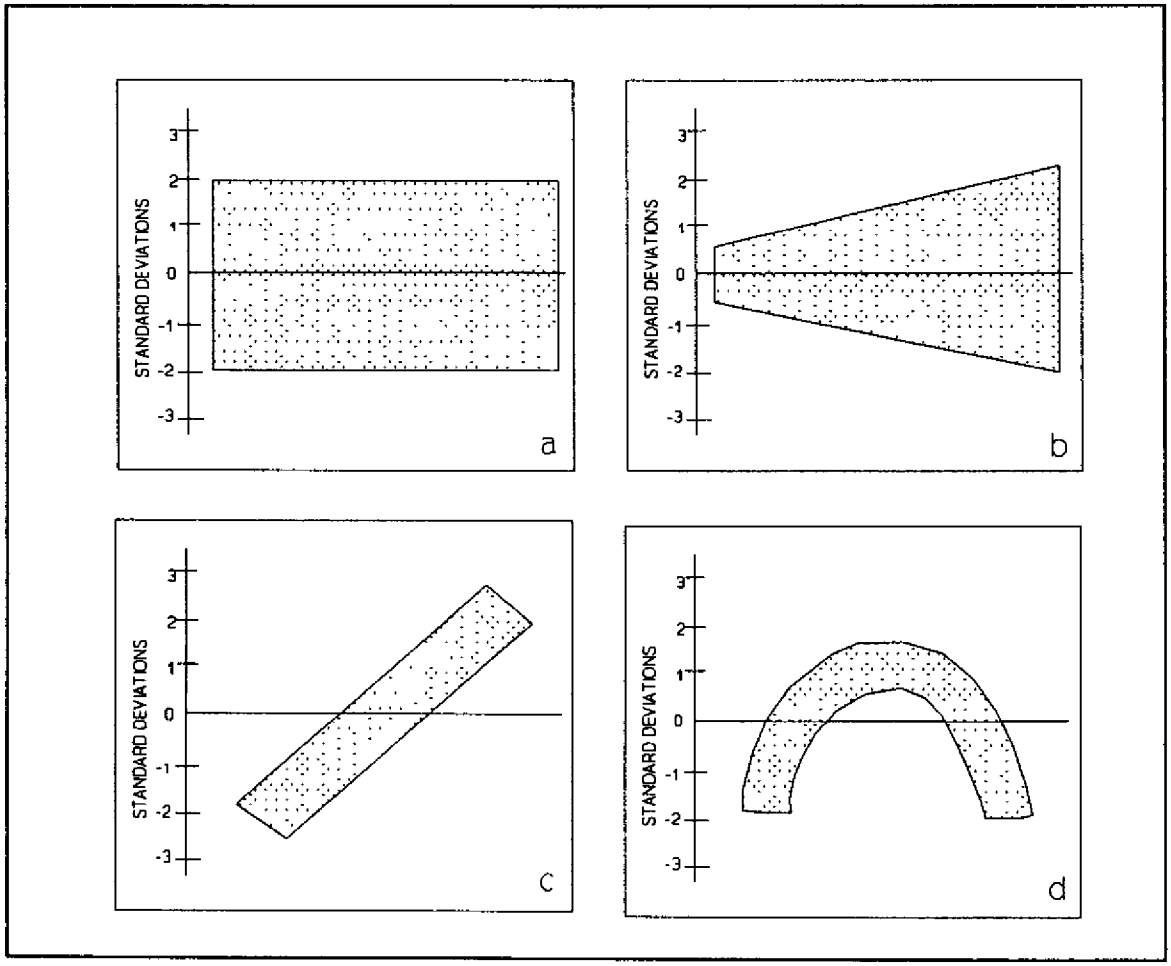

Figure 3-1 Examples of standard residual plots. **(a)** Satisfactory residual plot gives overall impression of horizontal box centered on zero line. **(b)** A plot showing nonconstant variance. **(c)** A plot showing a linear trend suggesting that the residuals are not independent and that another variable is needed in the model. **(d)** A plot illustrating the need for a transformation or a higher order term to alleviate curvature in the residuals.

Observations having $e_s(s)$ that plot more than 2 to 3 standard deviations above or below the zero line are potential outliers. Figures 3-1b through 3-1d are

examples of unsatisfactory residual plots. The behavior shown in Figure 3-1b suggests that the variance of $e_i(s)$ is not constant (i.e., the residual band widens). Data with a nonconstant variance are usually corrected by transforming Y or by using weighted, least-squares regression analysis (Draper and Smith, 1981). The linear trend shown in Figure 3-1c suggests that the $e_i(s)$ are not independent or that some other X is needed in the model. A residual plot displaying curvature (Figure 3-1d) indicates that a higher order term, a cross-product, or a transformation of Y, or of the X(s), is needed to produce a more linear form.

The performance of MLR models is judged by the coefficient of determination, R^2:

$$R^2 = [\Sigma(Y^2)-S_e-(\Sigma Y)^2/n]/[\Sigma(Y^2)-(\Sigma Y)^2/n)] \qquad (3.1.8)$$

where n is the sample size. The value of R^2 ranges from 0 to 1 and measures the proportion of the variability of Y being explained by the X(s). For example, a R^2 of 0.50 means that 50 percent of the variability in Y is being explained by the X(s).

In this study, we used a modified stepwise regression procedure to guide the development of our MLR models. In short, this procedure begins by searching the set of X(s) for the X with the highest correlation with Y and this X enters the model. In the next step, the remaining X(s) are re-examined to find the X that yields the next highest improvement in R^2 and this X is added to the model. The process of examining and adding X(s) to the model continues until no additional X can be found that significantly improves R^2. At the end of each step, partial t-tests are performed on all X(s) in the current model to verify that each X is still statistically significant. (Sometimes X(s) introduced during earlier steps become nonsignificant at later steps because they are correlated with other X(s) that are just entering the model). Variables that become nonsignificant during later steps are removed from the model prior to beginning the next step.

3.2 Compilation of Case History Data for MLR Analyses

Prior to beginning MLR analysis, 448 horizontal displacement vectors were compiled as the dependent variable, D_H, (m) from 8 earthquakes and the listed lateral spread sites in Table 3-1. Tabulated values of D_H were measured or estimated by the respective investigators using various methods. The values of D_H for Niigata and Noshiro, Japan, and the Jensen Filtration Plant were calculated from pre- and post-earthquake photographs using photogrammetric techniques (Hamada et al., 1986; O'Rourke et al., 1990). These measurements have an accuracy of ± 0.72, ± 0.17, and ± 0.47 m, respectively. The values of D_H for the Wildlife Instrument Array and Juvenile Hall were calculated from pre- and post-earthquake ground surveys (Youd, 1973b; Youd and Bartlett, 1988) and have an accuracy of approximately ± 0.02 m. The estimates of D_H at other lateral spread sites were obtained from reports of dislocated or offset buildings, bridge components, fences, canals, etc. The accuracy of D_H at these sites is difficult to determine, but is approximately ± 0.1 to ± 0.5 m.

Because of the large size of these data, the MLR database has been tabulated in ASCII format on the computer disk labeled "Appendix 3" in the file MLR.DAT. This disk and two additional disks, which comprise "Appendix 4", are available from NCEER Information Service, care of Science and Engineering Library, 304 Capen Hall, State University of New York at Buffalo, Buffalo, New York, 14260.

Table 3-2 lists the earthquake, topographical, geological, and soil independent variables that were compiled and tested in our MLR analyses. These data were obtained from seismological reports, topographical maps and surveys, borehole logs, and soil grain-size analyses (Appendix 1, 3, and 4). We used liquefaction susceptibility analysis of SPT data to calculate many of the geological and soil independent variables (Seed and Idriss, 1971; Seed et al., 1983; 1985, NRC 1985,

Liao, 1986). In all, liquefaction susceptibility analysis was performed for 267 boreholes from the lateral spread sites listed in Table 3-1 (Appendix 1 and 4).

TABLE 3-1
EARTHQUAKES AND LATERAL SPREAD SITES USED IN THIS STUDY

1906 San Francisco Earthquake (Youd and Hoose, 1978)

Coyote Creek Bridge near Milpitas, California
Mission Creek Zone in San Francisco, California
Salinas River Bridge near Salinas, California
South of Market Street Zone in San Francisco, California

1964 Alaska Earthquake (Bartlett & Youd, 1992; McCulloch & Bonilla 1970)

Bridges 141.1, 147.4, 147.5, 148.3, Matanuska River, Alaska
Bridges 63.0, 63.5, Portage Creek, Portage, Alaska
Highway Bridge 629, Placer River, Alaska (Ross et al., 1973)
Snow River Bridge 605A, Snow River, Alaska (Ross et al., 1973)
Bridges 3.0, 3.2, 3.3, Resurrection River, Alaska

1964 Niigata, Japan, Earthquake (Hamada et a. , 1986)

Numerous lateral spreads in Niigata, Japan

1971 San Fernando Earthquake

Jensen Filtration Plant, San Fernando, CA, (O'Rourke et al., 1990)
Juvenile Hall, San Fernando, CA, (Bennett, 1989; Youd, 1973b)

1979 Imperial Valley Earthquake (Bennett et al., 1984)

Heber Road near El Centro, California (Dobry et al., 1992)
River Park near Brawley, California

1983 Borah Peak Idaho, Earthquake

Whiskey Springs near Mackay, Idaho (Andrus and Youd, 1987)
Pence Ranch near Mackay, Idaho (Andrus et al., 1991)

1983 Nihonkai-Chubu Earthquake (Hamada et al., 1986)

Lateral spreads in the Northern Sector of Noshiro, Japan

1987 Superstition Hills Earthquake (Holzer et al., 1988; 1989)

Wildlife Instrument Array, Brawley, CA, (Youd and Bartlett, 1988)

At many sites, there was more than one borehole drilled within the zone of ground deformation (for example, see Figure 3-2). For these sites, we used an inverse-distance, linearly-weighted average to interpolate all geological and soil independent variables between boreholes. This averaging scheme assigns the largest weight to the borehole located closest to the displacement vector:

$$X_{AVG} = W_1*X_1 + W_2*X_2 + \ldots + W_i*X_n \quad (3.2.1)$$

where X_{AVG} is the weighted average, $X_1,\ldots,X_n$ are the corresponding values of **X** to be averaged for n boreholes, and $W_1,\ldots,W_n$ are the weights. These weights are calculated from:

$$Wi = 1/d_i / \Sigma(1/d_i) \quad (3.2.2)$$

where d_i is the distance from i^{th} borehole to the displacement vector of interest and $\Sigma(1/d_i)$ is summed for n boreholes (Appendix 1, Section A1.4). These weighted averages were calculated for each D_H prior to performing the regression analyses.

3.3 Strategy for Development of MLR Models

Because the earthquakes that generated lateral spreads in Niigata and Noshiro, Japan were seismically similar, we initially ignored the effects that **M**, **R**, **A**, and **D** have on displacement during preliminary model development. (Niigata and Noshiro incurred 7.5 and 7.7 magnitude earthquakes and were situated approximately 21 and 27 km from the zone of seismic energy release, respectively (Hamada, 1986; Mogi et al., 1964; Hwang and Hammack, 1984). By restricting our initial analyses to these two earthquakes, we were able to developed site-specific MLR models based solely on topographical, geological, and soil factors. Also, the extensive displacement and subsurface data for these two cities provided us with a large MLR database amenable to statistic analyses. (Three hundred and seventy seven (377) of the 448 tabulated displacement vectors are from Niigata and Noshiro). After developing site-specific models for Japan, we added the U.S. data to the analyses and adjusted the site-specific MLR models for a wider range of earthquake, topographical, and soil conditions not present in the Japanese data.

We observed two general types of lateral spread in Niigata: (1) lateral spread towards a free face, and (2) lateral spread down gentle ground slopes where a free face was not present. For example, Figure 3-2 shows the pattern of ground displacement along the banks of the Shinano River near the northern abutment of the Echigo Railway Bridge. The large and erratic displacements near the river obviously resulted from a lack of lateral resistance to deformation created by the incised channel. In contrast, ground deformation occurring north of the railroad embankment was smaller (a maximum of 2 m), more uniform, and directed away from the channel. Lateral spread in this area was not impacted by the channel, but resulted from movement down a gentle gradient that slopes 0.2 percent to the northeast. Our preliminary regression models for Niigata showed that the topographical regression coefficients fitted for free face failures differed significantly from those fitted for ground slope failures. Thus, we developed a separate MLR model for each type of failure. In Section 3.4, we discuss the development of a site-specific, free face model using data exclusively from Niigata. (No free face failures were identified in the study of Noshiro, Japan by Hamada et al., 1986). In Section 3.5, we discuss the development of a site-specific, ground slope model using ground slope failures from both Niigata and Noshiro. In Section 4.0, the U.S. case studies are included in the analyses and the MLR models are adjusted for a wider range of earthquake and site conditions.

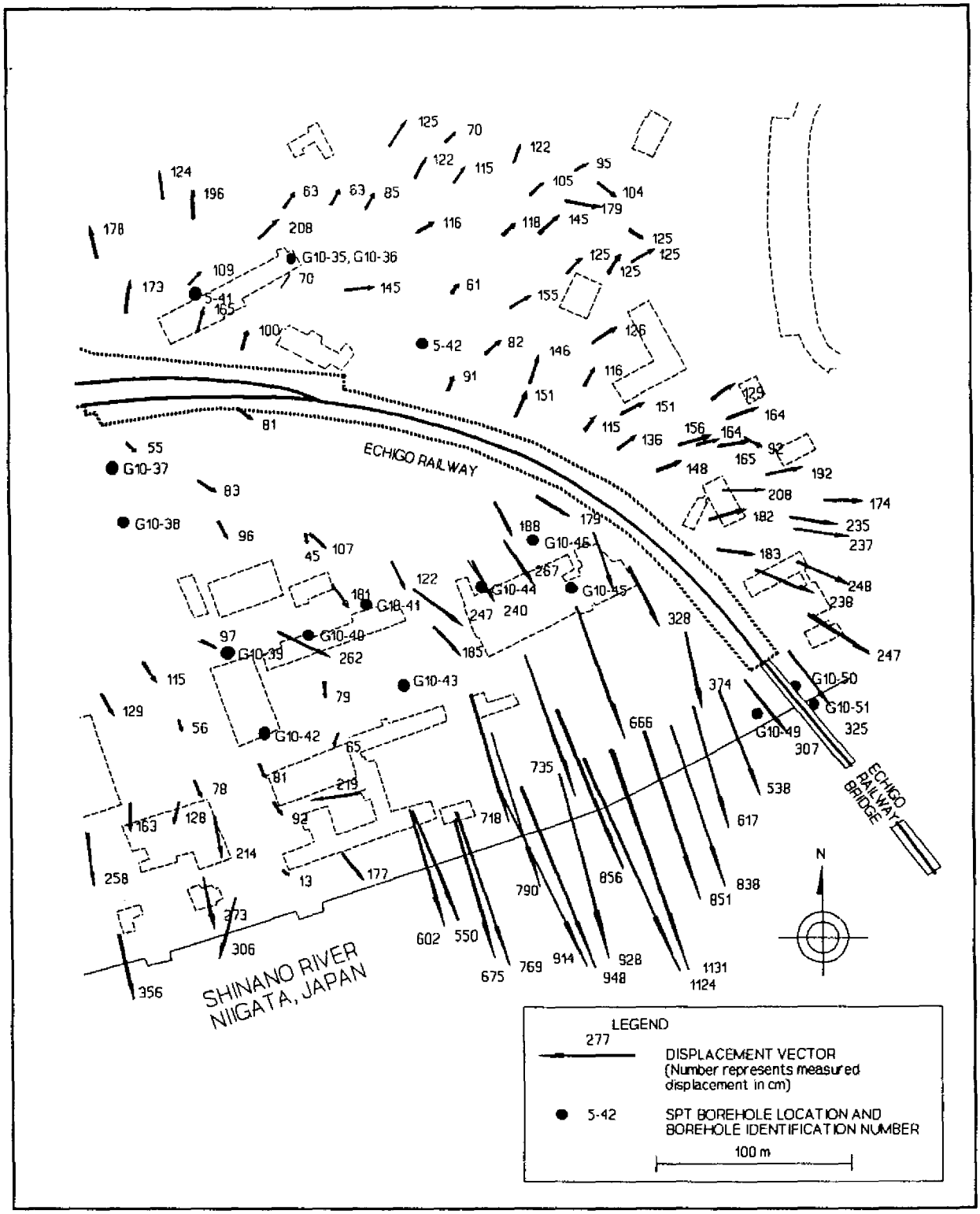

Figure 3-2 A section of working maps developed by Hamada et al. (1986), showing displacement vectors and locations of SPT boreholes from an area along the Shinano River near the Echigo Railway Bridge in Niigata, Japan (source: unpublished ground failure maps courtesy of M. Hamada).

TABLE 3-2
SUMMARY OF INDEPENDENT VARIABLES CONSIDERED IN MLR ANALYSIS
(For more information on these variables, see Section 4 and Appendix 1)

Earthquake Variables	Description
M*	Earthquake moment magnitude, M_w.
R*	Nearest horizontal distance to seismic energy source or fault rupture, (km).
A	Peak horizontal ground acceleration, (g).
D	Duration of strong ground motion (>0.05 g), (s).

Topographical Variables	Description
S*	Ground slope, (%).
L	Distance to the free face from the point of displacement, (m).
H	Height of free face, (m).
W*	Free face ratio, (%), (i.e., 100 H/L).

Geological Variables	Description
T_S	Thickness of liquefied zone(s) (Simplified procedure), (m).
T_L	Thickness of liquefied zone(s) (Liao's 50% probability curve), (m).
T_{10}	Thickness of saturated cohesionless soils with $(N1)_{60} \leq 10$, (m).
T_{15}*	Thickness of saturated cohesionless soils with $(N1)_{60} \leq 15$, (m).
T_{20}	Thickness of saturated cohesionless soils with $(N1)_{60} \leq 20$, (m).
I_S	Index of Liquefaction Potential (Simplified procedure).
I_L	Index of Liquefaction Potential (Liao's 50% probability curve).
Z_{tls}	Depth to top of liquefied zone (Simplified procedure), (m).
Z_{tll}	Depth to top of liquefied zone (Liao's 50% prob. curve), (m).
Z_{bls}	Depth to bottom of liquefied zone (Simplified procedure), (m).
Z_{bll}	Depth to bottom of liquefied zone (Liao's 50% prob. curve), (m).
Z_S	Depth to the lowest factor of safety (Simplified procedure), (m).
Z_L	Depth to the lowest factor of safety (Liao's 50% prob. curve), (m).
Z_N	Depth to lowest SPT N value in saturated cohesionless soil, (m).
Z_{N160}	Depth to lowest SPT $(N1)_{60}$ value in saturated cohesionless soil, (m).
N	Lowest SPT N value in saturated cohesionless sediments.
$N1_{60}$	Lowest SPT $(N1)_{60}$ value in saturated cohesionless sediments.
J_S	Lowest factor of safety below water table (Simplified procedure).
J_L	Lowest factor of safety below water table (Liao 50% prob. curve).
$N1_{60S}$	$(N1)_{60}$ value corresponding to J_S.
$N1_{60L}$	$(N1)_{60}$ value corresponding to J_L.
K_S	Average factor of safety in T_S.
K_L	Average factor of safety in T_L.
O_S	Average $(N1)_{60}$ in T_S.
O_L	Average factor of safety in T_L.

*** Indicates independent variables used in the final MLR model.**

TABLE 3-2 (CONTINUED)
SUMMARY OF INDEPENDENT VARIABLES CONSIDERED IN MLR ANALYSIS
(For more information on these variables, see Section 4 and Appendix 1)

Soil Variables	Description
$D50_S$	Average D_{50} in T_S, (mm).
$D50_L$	Average D_{50} in T_L, (mm).
$D50_{10}$	Average D_{50} in T_{10}, (mm).
$D50_{15}$*	Average D_{50} in T_{15}, (mm).
$D50_{20}$	Average D_{50} IN T_{20}, (mm).
F_S	Average fines content in T_S, (particle size <0.075 mm, in percent).
F_L	Average fines content in T_L, (particle size <0.075 mm, in percent).
F_{10}	Average fines content in T_{10}, (particle size <0.075 mm, in percent).
F_{15}*	Average fines content in T_{15}, (particle size <0.075 mm, in percent).
F_{20}	Average fines content in T_{20}, (particle size <0.075 mm, in percent).

*** Indicates independent variables used in final MLR model.**

3.4 Free Face MLR Model for Lateral Spreads in Niigata, Japan

Stepwise regression analyses of lateral spreads in Niigata show that the proximity of the channel is the most important site factor affecting ground displacement for free face failures. Figure 3-3 is a plot of horizontal displacement, D_H, (m), versus the horizontal distance from the channel, L, (m), for several lateral spreads along the Shinano River. This plot suggests that D_H decays logarithmically with increasing L. A regression of this single factor yields the following equation:

$$D_H = 11.6 - 4.38 \text{ LOG } L. \quad (3.4.1)$$

The R^2 for this model is 31.7 percent. Partial t-tests for the intercept, b_0, and the partial slope for LOG L are significant at the 99.9 percent confidence level (i.e., 99.9% probability that these coefficients are not equal to zero).

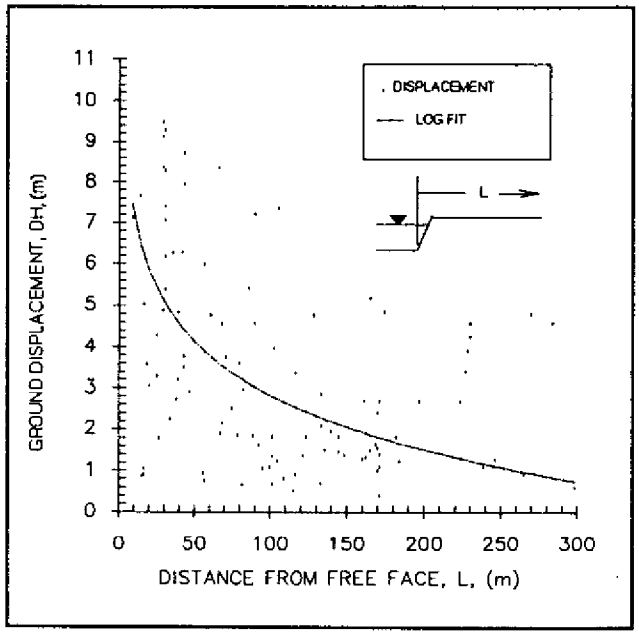

Figure 3-3 Plot of ground displacement, Y, versus distance from the free face, L, for lateral spreads along the Shinano River, Niigata, Japan.

In analyzing the ground deformation near the Shinano River, we noted that D_H near the bridge abutments appears to have been impeded by the structures. For example, Figure 3-2 shows that the displacement vectors near the north abutment of the Echigo railroad decreased from approximately 8 m (at a locality 75 m east of the bridge) to 3 m (at 10 m east of the bridge). In order to minimize the variability in D_H resulting from

bridge interference, we did not compile displacement vectors found within approximately 50 m of the bridges.

In addition to L, the height of the free face (i.e., the depth of the channel), H, (m), is also correlated with D_H. To normalize L for the effect of H, we combined these two topographic measures into one independent variable called the free face ratio, W, (%) (Figure 3-4):

$$W = 100\ H/L. \qquad (3.4.2)$$

Although there is considerable scatter due to other geological and soil factors not accounted for in the model, D_H appears to increase in a nonlinear fashion with W (Figure 3-4). To fit this nonlinearity, we tried the following models:

$$D_H = b_1\ SIN\ (H/L) \qquad (3.4.3a)$$

$$D_H = b_0 + b_1\ LOG\ W \qquad (3.4.3b)$$

$$LOG\ D_H = b_0 + b_1\ LOG\ W \qquad (3.4.3c)$$

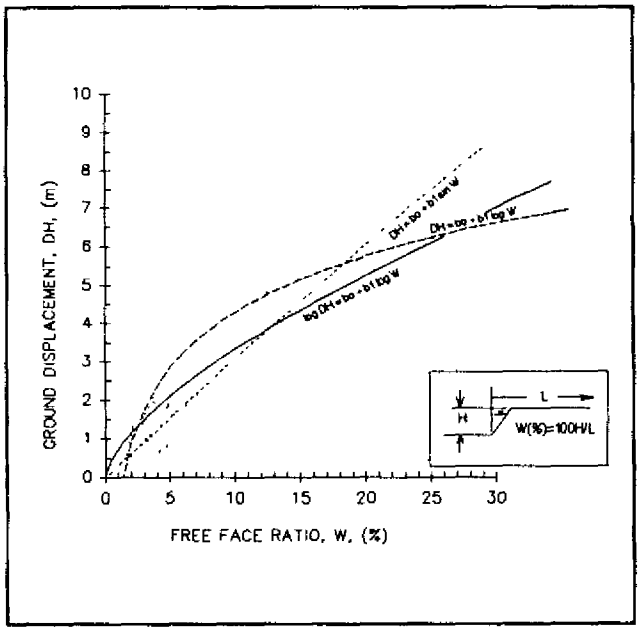

Figure 3-4 Plot of ground displacement, D_H, versus free face ratio, W, for lateral spreads along the Shinano River, Niigata, Japan.

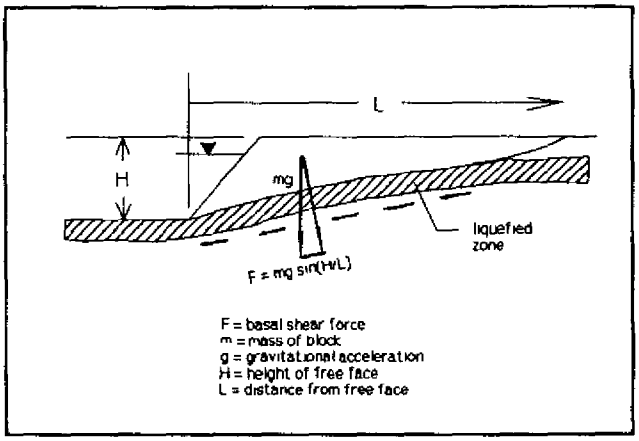

Figure 3-5 Diagram showing that the shear force acting along the base of slide block is proportional to sin (H/L).

Equation 3.4.3a is a plausible model for planar failure surfaces that intersect the free face. This model presupposes that D_H is proportional to the gravitational shear force acting along the base of the mobilized soil block (Figure 3-5). However, for the Niigata data, Equation 3.4.3a yielded poorer predictions compared with Equations 3.4.3b and 3.4.3c (R^2 equals 28.6 percent versus 39.1 and 38.0 percent, respectively).

A fit of model 3.4.3b yielded the highest R^2 value; but a residual plot of $e_i(s)$ versus D_{Hhat} from this model showed evidence of nonconstant variance. Figures 3-2 and 3-3 shows that D_H is more variable near the free face. This extra variability is most likely due to changes in the subsurface geology or is a result of impediments to displacement such as retaining walls, piles, and other buried structures found along the margins of the channel. Because MLR analysis assumes that the variance of e_i is constant throughout the ranges of the independent variables, nonconstant variance is undesirable and may pose problems in estimating the prediction limits for the true value of D_H. A log transformation of the dependent variable, Y, is a standard technique used to reduce nonconstant variance (Draper and Smith, 1981). Also, Hamada et al., 1986 and Youd and Perkins (1987) used log-log transformations similar to Equation 3.4.3c in their MLR models. Thus, we ultimately decided to transform D_H to LOG D_H (Figure 3-6) and fitted model 3.4.3c with the following coefficients:

$$\text{LOG } D_H = -0.138 + 0.660 \text{ LOG } W. \qquad (3.4.4)$$

A residual plot of $e_s(s)$ versus D_{Hhat} for Equation 3.4.4 indicates that the log-log model eliminates the nonconstant variance (Figure 3-7). The intercept and slope for this equation are highly significant. (The intercept is significant at the 97 percent confidence level and the slope for LOG W is significant at the 99.9 percent confidence level.)

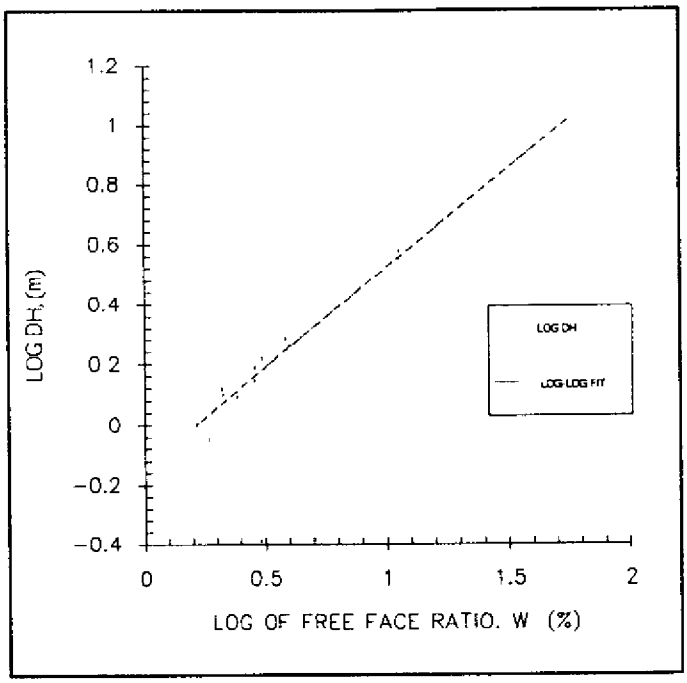

Figure 3-6 Plot of LOG D_H versus LOG W for lateral spread displacements along the Shinano River, Niigata, Japan showing an approximately linear relationship.

In analyzing free face failures near the Shinano River in Niigata, we postulated that the slope of the river bank into or away from the channel may have had an effect on D_H and we tabulated and tested a second variable, S, (%), to represent that possible effect. The value of S was assigned a positive value for cases where the ground sloped toward the channel (Figure 3-8, Case 1) and a negative value for cases where the ground sloped away from the channel (Figure 3-8, Case 2). The inclusion of S in the free face model did not improve R^2 significantly; hence, we concluded that the slope of the floodplain near the Shinano River does not vary enough to have markedly affected D_H. In general, we found this conclusion to be true for other case history sites where free face failures occurred near major river channels.

We also adjusted the free face model for the effects of subsurface geology and soil conditions. Stepwise regression indicated that the cumulative thickness of the liquefied layer, T, (m), is the next variable that should enter the model. Some modelers have used liquefaction analyses based on empirical curves and SPT $(N1)_{60}$ values to estimate T (Seed and Idriss, 1971; Seed et al., 1983, 1985; NRC, 1985; Hamada, 1986; Liao, 1986). However, these techniques require an estimate of the earthquake magnitude, M, and peak ground acceleration, A, as input into the analyses. Thus, T determined from these methods will be correlated with the earthquake factors M and A. To minimize the correlation between earthquake and site factors, we defined and tested three estimates of T that are calculated without performing

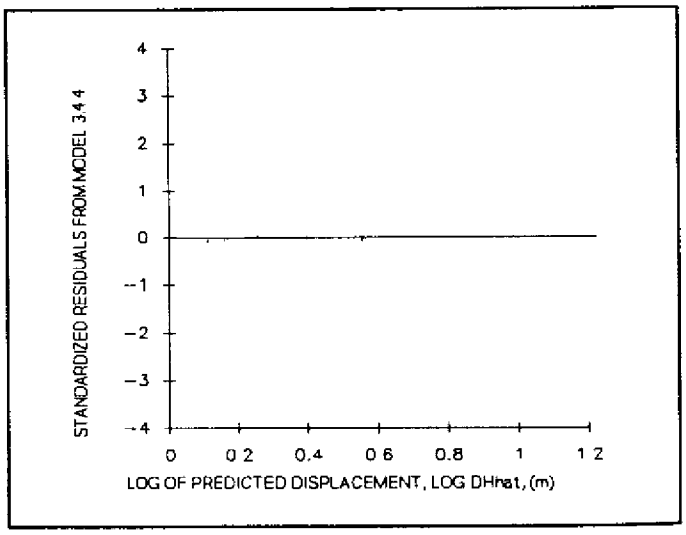

Figure 3-7 Standardized residuals, e_s's, from model 3.4.4 plotted against LOG D_H showing no evidence of nonconstant variance.

liquefaction analyses. We defined T_{10}, T_{15}, and T_{20} as the cumulative thickness, (m), of saturated cohesionless sediments with SPT $(N1)_{60}$ values ≤ 10, 15, and 20, respectively. Saturated soils with a clay content ≥ 15 percent were not added to these cumulative thickness. Also, because most boreholes included in our study were drilled to a maximum depth of 20 meters, T_{10}, T_{15}, and T_{20} were generally accumulated in the upper 20 m of the soil profile. The substitution of T_{10}, T_{15}, and T_{20} for T into the free face model:

$$\text{LOG } D_H = b_0 + b_1 \text{ LOG } W + b_2 T. \qquad (3.4.5)$$

yields R^2 values of 50.9, 62.4, and 63.8 percent, respectively. We ultimately chose to use T_{15} instead of T_{20} in all subsequent models because our case history data suggests that lateral spreads are generally restricted to deposits having $(N1)_{60}$ values ≤ 15 for M ≤ 8.0 earthquakes. A plot of the ε_s(s) from model 3.4.4 versus T_{15} shows an approximately linear relationship between LOG D_H and T_{15} (Figure 3-9a), thus we formed the model:

$$\text{LOG } D_H = -0.537 + 0.568 \text{ LOG } W + 0.0458\ T_{15}. \qquad (3.4.6)$$

All regression coefficients for this model are significant at the 99.9 percent confidence level.

After adjusting the free face model for the influence of W and T, stepwise regression indicated that the percentage of fines, F, (particle size ≤ 0.075 mm) of the liquefied layer is the next variable that should enter the free face model. In Figure 3-9b, the ε_s(s) from Equation 3.4.6 are plotted against the average fines content in T_{15}. The linear trend implies that horizontal displacement decreases with increasing fines content. The free face model adjusted for F is:

$$\text{LOG } D_H = -0.355 + 0.594 \text{ LOG } W + 0.0369\ T_{15} - 0.0102\ F_{15} \qquad (3.4.7)$$

where:
F_{15} = average fines content in T_{15}, in percent.

The R^2 for this model is 66.0 percent and all regression coefficients are significant at the 99.9 percent confidence level.

The mean grain size, D_{50}, (mm), of the channel deposits along the Shinano River also had a minor influence on displacement. In Figure 3-9c, the ε_s(s) from model 3.4.7 are plotted against the average D_{50} in T_{15}. Although showing considerable scatter, this plot suggests that displacement decreases as the average D_{50} value in T_{15} increases. Model 3.4.7 adjusted for D_{50} is:

$$\text{LOG } D_H = 0.301 + 0.563 \text{ LOG } W + 0.0338\ T_{15} - 0.0244\ F_{15} - 1.50\ D50_{15} \qquad (3.4.8)$$

where:
$D50_{15}$ = average D_{50} in T_{15}, in millimeters.

The R^2 for this model is 70.0 percent and partial t-tests show that intercept is significant at the 90 percent confidence level and all other regression coefficients are significant at the 99.9 percent confidence level.

In addition to $D50_{15}$, the $(N1)_{60}$ value associated with the lowest factor of safety against liquefaction in the liquefied profile, $N1_{60S}$, makes a minor contribution to improving the performance of the free face model. The value of R^2 increased from 70.0 to 72.4 percent as $N1_{60S}$ was included. To determine $N1_{60S}$, a factor of safety against liquefaction, FS, was calculated for each $(N1)_{60}$ value in the profile by applying the "simplified procedure" for liquefaction analysis (Seed

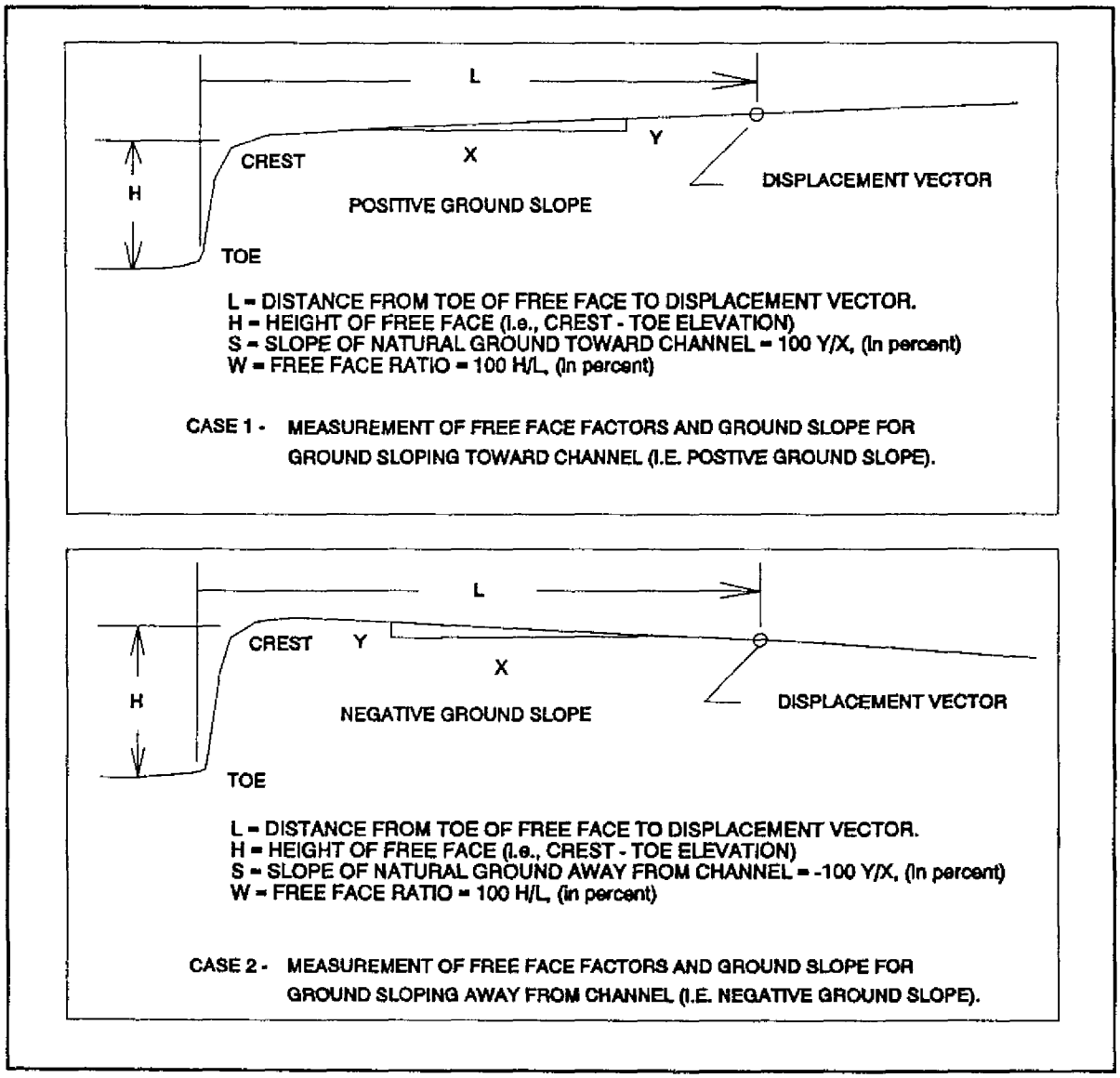

Figure 3-8 Definition of free face factors, L and H, and ground slope, S, for free face failures.

and Idriss, 1971; Seed et al., 1983; 1985; see also Appendix 1):

$$FS = CSRL/CSRQ \qquad (3.4.9)$$

where:
CSRL = cyclic stress ratio required for liquefaction
CSRQ = cyclic stress ratio induced in the profile by the earthquake.

The $(N1)_{60}$ value corresponding to the lowest **FS** in the profile was assigned to $\mathbf{N1_{60S}}$. The $\mathbf{e_v(s)}$ from Equation 3.4.8 plotted against $\mathbf{N1_{60S}}$ indicate that displacement tends to decrease with increasing values of $\mathbf{N1_{60S}}$ (Figure 3-9d).

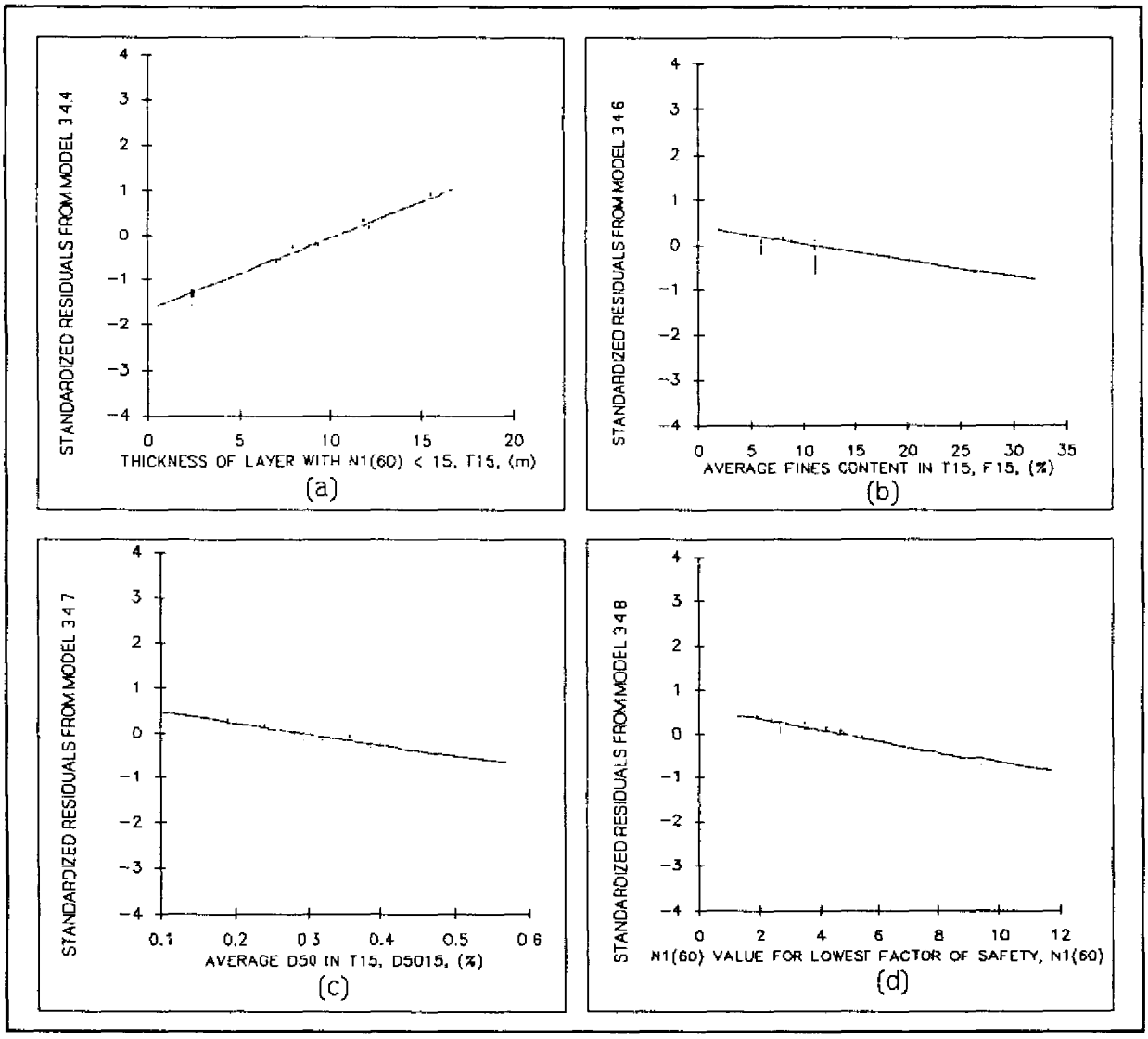

Figure 3-9 (a) Standardized residuals from model 3.4.4 plotted against the thickness of saturated cohesionless sediments with SPT $(N1)_{60}$ values ≤ 15, T_{15}, showing a linear relationship between T_{15} and e_s. **(b)** Standardized residuals from model 3.4.6 plotted against the average fines content, F_{15}, in T_{15} showing a linear relationship between F_{15} and e_s. **(c)** Standardized residuals from model 3.4.7 plotted against the average mean grain size, $D50_{15}$, in T_{15} showing a linear relationship between $D50_{15}$ and e_s. **(d)** Standardized residuals from model 3.4.8 plotted against the SPT $(N1)_{60}$ value corresponding to the lowest factor of safety in the liquefied profile, $N1_{60s}$, showing a linear relationship between $N1_{60s}$ and e_s.

The addition of $N1_{60s}$ in the free face model yields:

$$\text{LOG } D_H = 0.610 + 0.572 \text{ LOG } W + 0.0247\ T_{15} - 0.0278\ F_{15} - 1.61\ D50_{15} - 0.0315\ N1_{60s} \qquad (3.4.10)$$

The inclusion of other possible geological and soil factors from Table 3-2 in Equation 3.4.10 did not appreciably improve the performance of the model; thus, this equation was adopted as the final model for free face failures in Niigata.

We did obtain a slightly higher R^2 values by including interaction terms in the model (i.e., cross-products of LOG W, T_{15}, F_{15}, $D50_{15}$, and $N1_{60s}$), but the physical

meanings of these interactions were difficult to interpret. Thus, we do not believe that the slight improvement in R^2 warrants the addition of higher order terms and we formulated all of our subsequent models with first order terms only.

All regression coefficients for Equation 3.4.10 are significant at 99 percent confidence level. Appendix 2 contains the MINITAB printout for this model (Minitab, 1989; Ryan et al., 1985). This output lists the regression coefficients, their standard deviations, partial t-tests for significance, an analysis of variance (ANOVA) table, and a list of potential outliers. The standardized residual plots for this model are also given in Appendix 2.

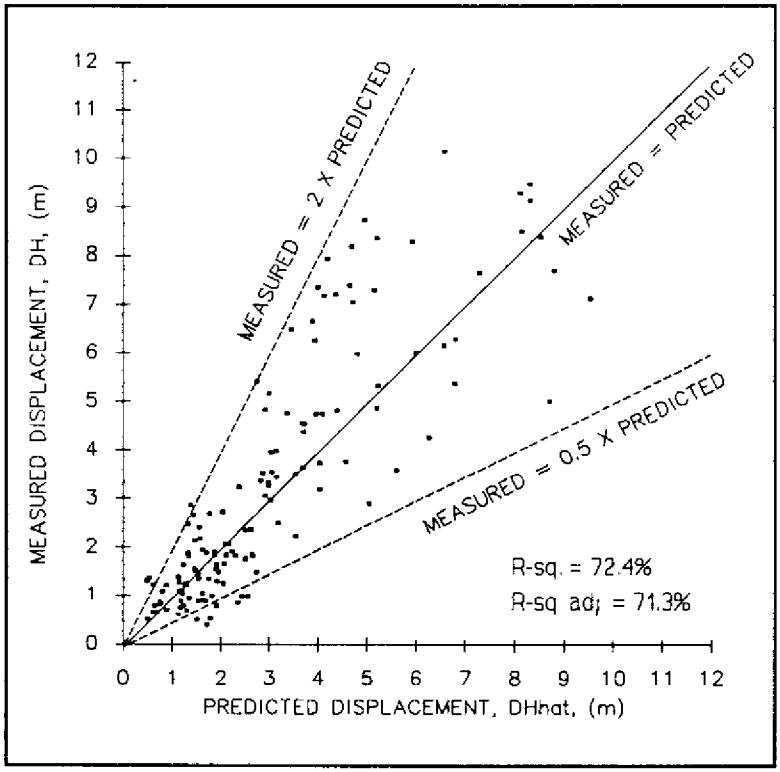

Figure 3-10 Plot of measured displacements, D_H, versus predicted displacements, D_{Hhat}, for Equation 3.4.10, Shinano River, Niigata.

In addition to evaluating R^2, a plot of D_H versus D_{Hhat} provides a simple way to view the predictive performance of this model (Figure 3-10). The solid "MEASURED = PREDICTED" line represents a perfect prediction line. Observations plotting near this line are closely approximated by the regression model. The dashed line below the "MEASURED = PREDICTED" line represents a 100 percent overprediction bound. Observations plotting below this line are being overpredicted by a factor of two or greater. The dashed line above the "MEASURED = PREDICTED" line is a 50 percent underprediction bound. Observations falling above this line are being underpredicted by a factor of two or greater. In summary, 92 percent (128 out of 139) of the displacements predicted by Equation 3.4.10 fall between these upper and lower prediction bounds.

3.5 Ground Slope Model for Niigata and Noshiro, Japan

Stepwise regression indicated that ground slope, **S**, is highly correlated with D_H for ground slope failures in Niigata and Noshiro, Japan. In Niigata, lateral spread occurred on very gentle, uniform slopes ($S \leq 1$ percent); whereas, in Noshiro, lateral spread developed on undulating, dune deposits with slopes that are as steep as 5 percent in some locales. Because of the undulating topography found in Noshiro, we used slightly different techniques to measure **S** for uniform and nonuniform slopes. Figure 3-11, Case 1 shows the technique we used to measure **S** for the long, uniform slopes that were typical of Niigata. The value of S, (%), for these cases was calculated simply as:

$$S = 100\ Y/X. \qquad (3.5.1)$$

However, in Noshiro, the amount of ground displacement was strongly influenced by undulations in the sand dunes. For example, Figure 3-12 shows that the ground displacement tended to mirror the topography, increasing near the steeper part of the undulating dune and decreasing in more gentle reaches. From the observed

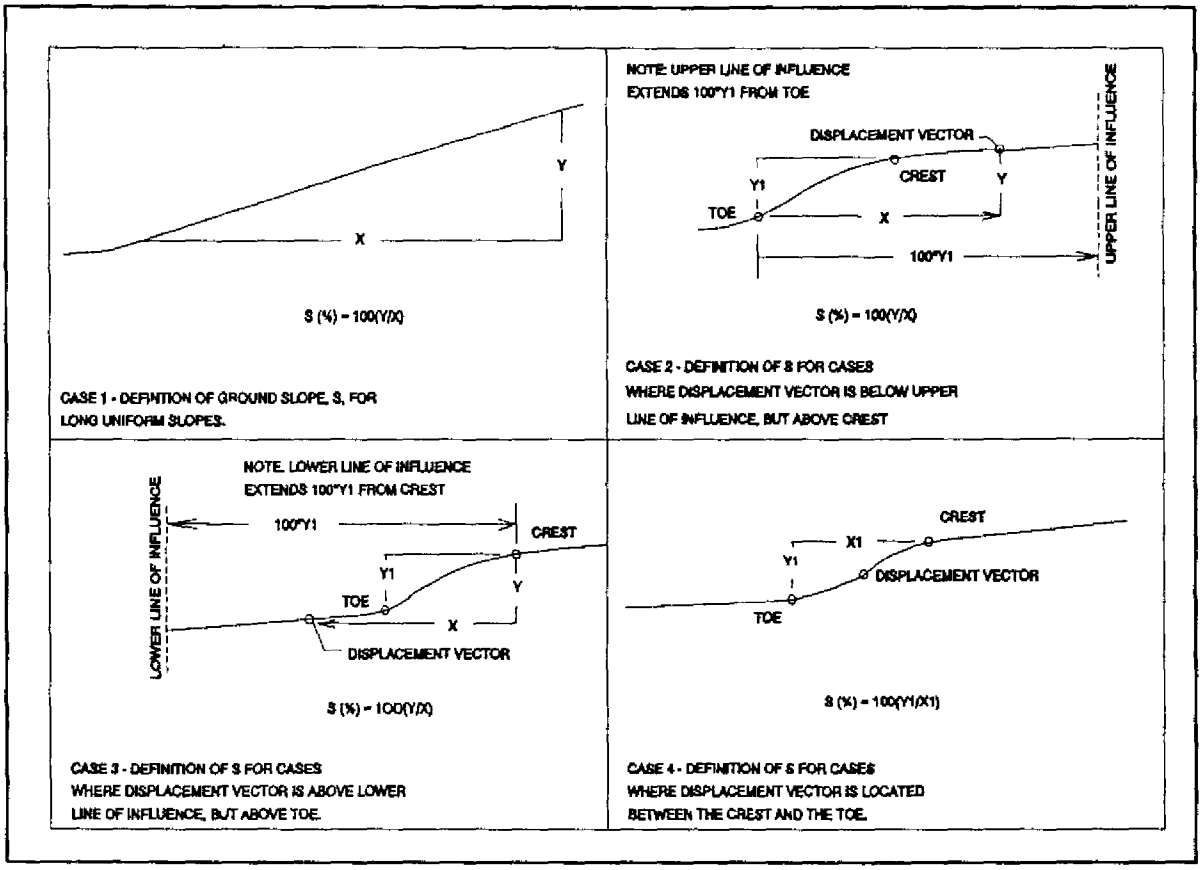

Figure 3-11, Case 1. Definition of ground slope, S, for long uniform slopes. **Cases 2 - 4.** Definition of S for nonuniform slopes.

displacement pattern, we noted that the zone of increased displacement near the undulations generally extended above and below the toe and crest of the undulations for a maximum horizontal distance of approximately 100 times the height of the undulation. Thus, our measurements of **S** for displacement vectors falling within this zone were steepened to either the crest or to the toe of the undulations as shown in Figure 3-11, Cases 2 and 3. Figure 3-11, Case 2 shows the definition used to measure **S** for displacement vectors that occurred above the crest of the undulations, but within 100 Y_1 of the toe of the undulations. Figure 3-11, Case 3 shows the definition used to measure **S** for vectors that were located below the toe of the undulations, but within 100 Y_1 of the crest of the undulations. Figure 3-11, Case 4 shows the definition used to assign **S** to all vectors located on the face of the undulations. We applied these same techniques to measure **S** for all undulating slopes found in our study.

As was discovered in developing the free face model, regression analyses of ground slope failures in Niigata and Noshiro indicate that a model comprised of **LOG** D_H and **LOG S** produces an approximately linear form (Figure 3-13):

$$\text{LOG } D_H = 0.430 + 0.442 \text{ LOG } S. \qquad (3.5.2)$$

The R^2 for this model is 42.1 percent. The regression coefficients for this model are significant at the 99.9 percent confidence level.

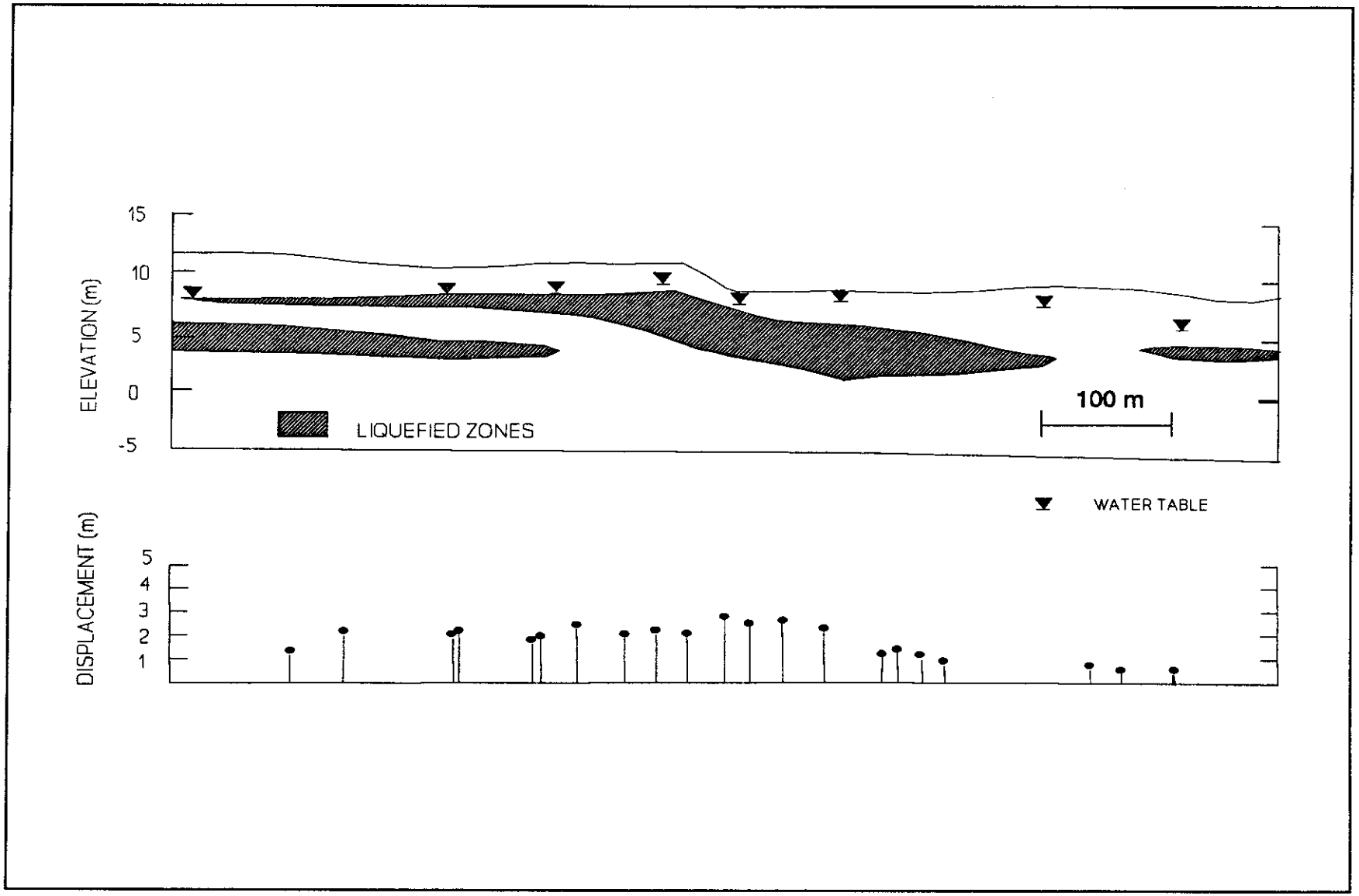

Figure 3-12 Typical topography and ground displacement pattern for ground slope failures in Noshiro, Japan, (after Hamada et al., 1986).

A slightly better fit (R^2 = 45.6%) was obtained by forming the model: $D_H = b_0 + b_1$ LOG S, but like the free face model, a plot of $e_i(s)$ versus D_{Hhat} suggested a slight problem with nonconstant variance. Also, because we transformed D_H to LOG D_H in developing the free face model, it was beneficial to maintain the same functional form in developing the ground slope model. This will allow us to combine both models into a single regression operation as the earthquake factors are brought into the analyses (for further discussion, see the next section).

As was discovered in developing the free face model, the variables T_{15}, $D50_{15}$, and F_{15} also contribute to improving the performance of the ground slope model. Furthermore, like the free face model, standardized residuals from model 3.5.2 plotted against T_{15}, $D50_{15}$, and F_{15} suggest that the relationships between displacement and these variables are approximately linear, thus these factors were also included in the ground slope model:

$$\text{LOG } D_H = 0.698 + 0.378 \text{ LOG S} + 0.0362\ T_{15} - 0.0326\ F_{15} + 0.929\ D50_{15}. \quad (3.5.3)$$

No additional geological and soil factors substantially improved this model, thus it was adopted as the final model for predicting ground slope failures in Niigata and Noshiro. The R^2 for Equation 3.5.3 is 54.2 percent and the intercept and regression coefficients are significant at the 99 percent confidence level (see MINITAB output in Appendix 2). A plot of D_H versus D_{Hhat} for this model shows that 97 percent (224 out of 232) of the predicted displacements fall between the 100 percent overprediction and 50 percent underprediction bounds (Figure 3-14).

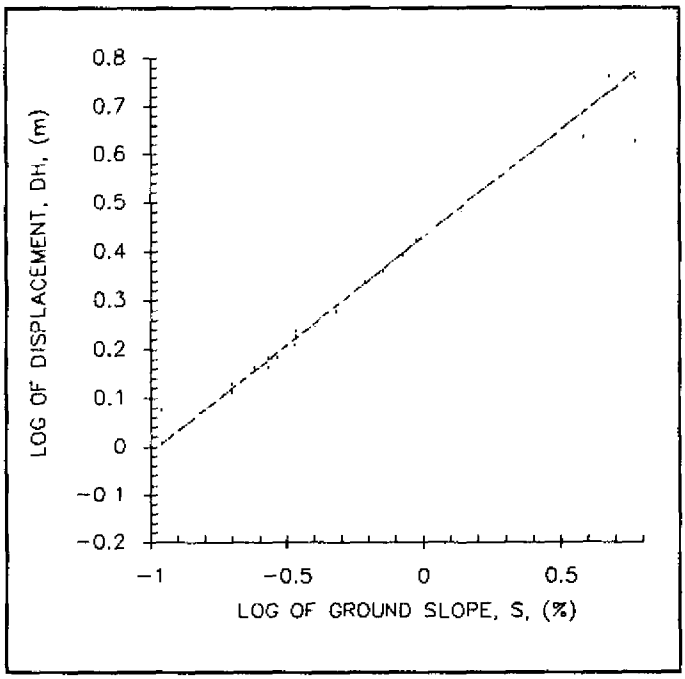

Figure 3-13 Plot of log of displacement, LOG D_H, versus log of ground slope, LOG S, for ground slope failures indicating an approximately linear trend.

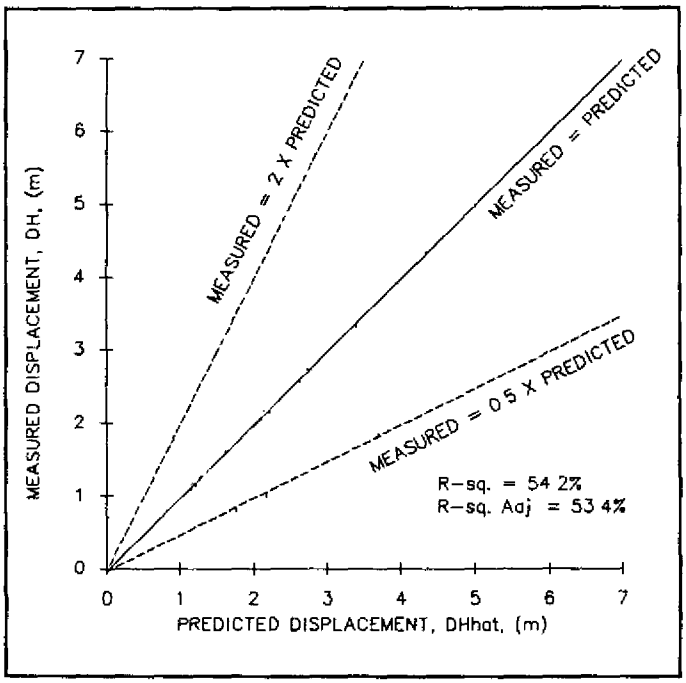

Figure 3-14 Plot of measured displacements, D_H, versus predicted displacements, D_{Hhat}, for Equation 3.5.3, ground slope failures, Niigata and Noshiro.